Materials Research Express

PAPER

$La_{0.59}Li_{0.24}TiO_3$ ceramics obtained by spark plasma sintering: electric behavior analysis

To cite this article: J S Pereira *et al* 2019 *Mater. Res. Express* **6** 015504

View the article online for updates and enhancements.

IOP ebooks™

Bringing you innovative digital publishing with leading voices to create your essential collection of books in STEM research.

Start exploring the collection - download the first chapter of every title for free.

This content was downloaded from IP address 129.186.138.35 on 23/01/2019 at 13:08

Materials Research Express

PAPER

$La_{0.59}Li_{0.24}TiO_3$ ceramics obtained by spark plasma sintering: electric behavior analysis

RECEIVED
29 August 2018

REVISED
24 September 2018

ACCEPTED FOR PUBLICATION
27 September 2018

PUBLISHED
10 October 2018

J S Pereira[1], F. Guerrero[1], Y Romaguera-Barcelay[1], J Anglada-Rivera[2], J C C Sales Jr[3], R S Silva[4], Y Zulueta[5], R Poyato[6], A Gallardo[7], A Almeida[8], J Agostinho Moreira[8] and Y Leyet[1,3]

[1] Departamento de Física, Universidade Federal do Amazonas, 69077-000, Manaus, AM, Brasil
[2] Instituto Federal de Educação Ciência e Tecnologia do Amazonas, 69020-120, Manaus, AM, Brasil
[3] Departamento de Engenharia de Materiais, Universidade Federal do Amazonas, 69077-000, Manaus, AM, Brasil
[4] Departamento de Física, Universidade Federal de Sergipe, 49100-000, São Cristóvão, SE, Brasil
[5] Departamento de Física, Universidad de Oriente, 90300, Santiago de Cuba, Cuba
[6] Inst. Ciencia de Materiales de Sevilla (CSIC-Univ. de Sevilla), 41092 Sevilla, España
[7] Dpto. de Física de la Materia Condensada, ICMS, CSIC- Universidad de Sevilla, 41080 Sevilla, España
[8] IFIMUP-IN, Institut of Nanoscience and Nanotechnology, Departamento de Física e Astronomia. Faculdade de Ciências da Universidade do Porto, 4169-007 Porto, Portugal

E-mail: yurileyet@yahoo.es

Keywords: lithium lanthanum titanate, SPS, solid state electrolytes

Abstract

This work describes the electric study of Lithium lanthanum titanate ($La_{0.59}Li_{0.24}TiO_3$) ceramics performed by Complex Impedance Spectroscopy. The nanoparticle powders have been synthesized through high energy ball milling and sintered via Spark Plasma Sintering technique. The experimental impedance data have been analyzed using the equivalent circuit model, the Extended Jonscher universal law and the derivative method. From these models, we have determined the dielectric response as well as the grain and grain boundary conductivity. The samples show ionic conductivity values between 10^{-5} to 10^{-4} S cm^{-1} in the studied temperature range, and activation energy values 0.24 eV and 0.48 eV for grain and grain boundary, respectively. These results confirm the Li^+ ions mobility through the crystalline structure of the material.

1. Introduction

The batteries of organic liquid electrolytes with lithium ion (Li^+) carriers are inflammable and susceptible to auto ignition [1]. This fire hazard can be due to the internal short circuit caused by physical damages after mechanical impacts, heating above room temperature, or internal defect production [1–4]. Incidents caused by such malfunctions are of extreme concern due to personal transportation vehicles and large commercial aircraft safety [4]. With this concern in mind, several authors have been proposing to replace organic liquid electrolytes by solid state ones, since the latter convey better characteristics regarding safety hazard [1, 3, 5–7].

Some inorganic solid state electrolytes present higher ionic conductivity (10^{-3} to 10^{-4} S cm^{-1}) at room temperature, as well as, good chemical stability [1, 8]. Other advantages are, for instance, the decrease of batteries heating, the larger durability, corrosion elimination [1, 5]. Among these solid state electrolytes, the materials based on lithium awake great interest due to their possible application in high energies batteries and electrochemical devices [1, 2, 8].

Among lithium-based solid state electrolytes, the solid electrolyte lithium lanthanum titanate, $La_{(2/3-x)}Li_{3x}TiO_3$ (LLTO), with perovskite structure, has been extensively studied [1, 6, 8, 9]. It has relatively high intrinsic conductivity at room temperature, reaching values up to 10^{-3} S cm^{-1} [1, 9–11]. The high conductivity values obtained in LLTO can be associated with its crystalline structure (opened, stable and rigid, having empty and accessible positions for the Li^+ ion), as well as, with the small mass and size of the Li^+ carrier that facilitates its conduction [9].

© 2018 IOP Publishing Ltd

Complex impedance spectroscopy (CIS) is a technique used to characterize solid insulating materials [5, 12]. In this technique, complex impedance measurements (Z^*) are performed as a function of the frequency, while the temperature is kept constant. [13]. The obtained results carry information regarding some key characteristics of the material, as conductivity, relaxation time, permittivity, and resistance and capacitance of the electrolyte/electrode interface [12, 14].

In many cases only the total conductivity of the material is presented, without giving details of the grain's contribution and the effect of its grain boundary. This study is of great importance because it allows a better understanding of the processes and phenomena that occur in a given material. In the analysis of the electric response through CIS, the Nyquist diagram (Z' versus Z') [1, 14] is usually used, since it allows to obtain the parameters of the circuits (resistances, capacitances, phase elements of constant phase, etc.) using the equivalent circuit (EC) model. This model enables us to separate the different contributions to the conductivity (grain, grain boundary) [12, 13, 15]. This model consists of assembling a circuit whose electrical response is similar to that of the experimentally obtained samples [12].

As far as we know, in the literature there are just a few publications on the X = 0.08 composition sintered by Spark Plasma Sintering (SPS). This work reports a detailed study of the electrical response of $La_{0.59}Li_{0.24}TiO_3$ (LLT) ceramics sintered by SPS. The equivalent circuit model, extended Jonscher universal law and derivative method (DM) were used to analyze the data obtained from Complex Impedance Spectroscopy measurements (CIS). From those models, the electrical conductivity values were calculated, and the different contributions to the conduction mechanism are discussed.

2. Materials and methods

The LLT nanopowders were produced by high energy ball-milling technique using La_2O_3(*Aldrich* −99.9%), Li_2CO_3 (*Aldrich* −99.9%) and TiO_2 (*Aldrich* −99.7%) as precursor materials. The precursors were ball-milled in a planetary system using steel spheres with 15 mm diameter, with 400 rpm milling speed for 40 h. The powders were compacted in disk form and sintered by the SPS (Dr Sinter Inc. model 515S, Kanagawa, Japan) [16, 17]. More details of the synthesis and sintering processes used can be seen in reference [18]. After sintering the samples were thermally treated at 850 °C for 3 h to promote the samples process of re-oxidation.

The structural characterization was carried out using a Rigaku D-max diffractometer, using Cuk_α radiation, in continuous mode, from 10° to 90° in 2θ. The unpolarized micro-Raman spectra were recorded at room conditions using an excitation line of 514.5 nm from Ar^+ laser, at 15 mW, in order to avoid local heating, and a 100x objective lens. The spectral slit width is ~1.5 cm^{-1}. The scattered light was analyzed with a Jobin-Yvon T64000 spectrometer and the spectra recorded with a LN2 cooled CCD.

The CIS measurements were carried out between 25 °C and 270 °C, and in a frequency range from 100 Hz to 10 MHz, with an applied potential of 500 mV. The data were registered using a Solartron 1260 Impedance Analyzer coupled to a Solartron 1296A dielectric interface, controlled by a personal computer. Electrical contacts were formed on both major surfaces of the polished ceramic by applying Pt paste, and then fired at 700 °C for 30 min.

3. Results and discussion

Figure 1(a) shows the x-ray diffraction pattern of the LLT ceramics, indexed [1, 9] as tetragonal phase, P4/mmm space. Additional peaks corresponding to $Li_4Ti_7O_{16}$ secondary phase are also identified. The total contribution of the secondary phase was 18%. The lattice parameters for the LLT phase were determined using the Le Bail model, being a = b = 3.88 Å and c = 7.78 Å, whose uncertainty values are less than 3% as compared with references [1, 9, 19].

The room-temperature unpolarized Raman spectrum of the LLT ceramic, in the 100–650 cm^{-1} spectral range, is shown in figure 1(b). The spectrum could be deconvoluted into 9 main bands, whose wavenumbers agree with the those already reported for this material [20–22]. The bands located at 140, 234, and 521 cm^{-1} have E_g symmetry, whereas the bands located at 315, 448, 557, and 580 cm^{-1} have A_{1g} symmetry. The band at 140 cm^{-1} involves mostly the motion of the Ti^+ cations and is therefore assigned to in-plane Ti^+ vibrations. The band at 234 cm^{-1} is assigned to the O-Ti-O bond bending mode. The band at 315 cm^{-1} corresponds to Ti^+ motions along the *c* axis, while the band at 448 cm^{-1} is associated with oxygen vibrations. The band at 521 cm^{-1} seems more likely due to Ti-O bond stretching. The two high-frequency components at 557 and 580 cm^{-1} consist of basically O(3) motion along the *c* axis, perturbed by the presence of nearby lithium atoms. These bands are compatible with the tetragonal P4/mmm structure, evidenced from analysis of the x-ray pattern. Finally, the Raman bands at 108, 166 and 376 cm^{-1}, have not been reported yet [20–22], and probably emerge from the second phase, already observed in the x-ray spectrum (figure 1(a)).

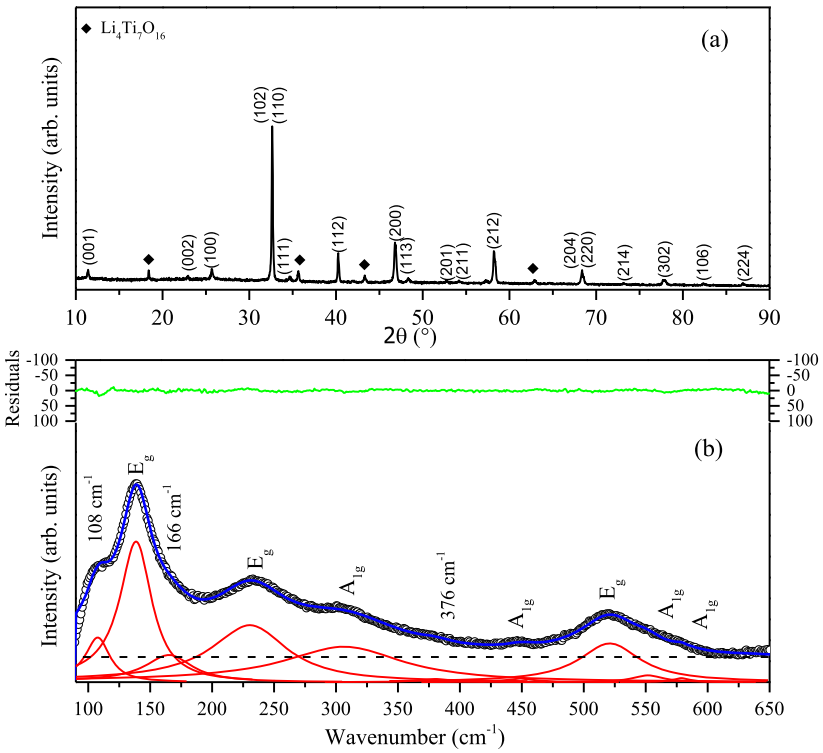

Figure 1. (a) XRD pattern and b) Raman spectrum of the LLT ceramic measured at room temperature. The peaks marked with (◆) correspond to a $Li_4Ti_7O_{16}$ secondary phase.

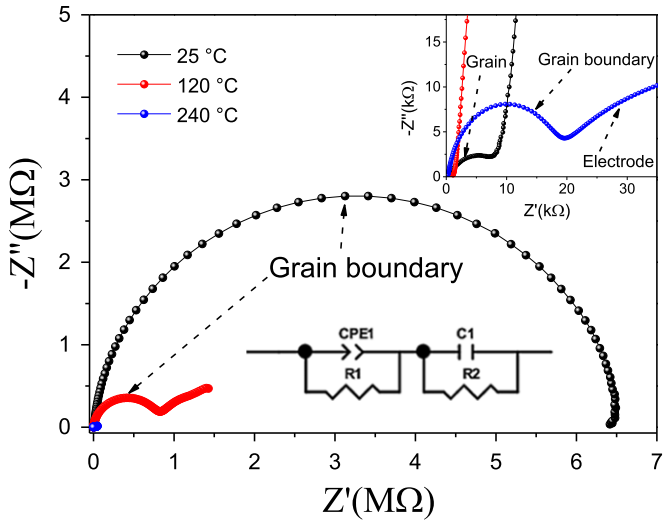

Figure 2. The (-Z′ versus Z′) Nyquist diagrams, measured at 25 °C, 120 °C and 240 °C. Upper insert: Nyquist diagram corresponding to the low frequencies region obtained at 25 °C and 120 °C and the second semicircle for 240 °C. Lower insert: circuit diagram used in the fitting procedure.

Figure 2 shows the Nyquist diagram (Z′ versus -Z′) of the LLT ceramic measured at 25 °C, 120 °C and 240 °C. It is possible to observe a large semicircle (low frequency region), due to grain boundary response, and a much smaller one (high frequency region), caused by the grain response (detail in figure 2). This behavior is characteristic of a material with heterogeneous electric response, semiconductor grain and insulating grain boundary [23].

Using the EC method, the proposed circuit to represent the sample behavior (lower inset in figure 2) is formed by two circuits in series, each composed of a resistor (R) in parallel with an another component: One with a capacitor (C1—grain boundary), and the other with a constant-phase element (CPE—grain) [12]. Using

Table 1. Total conductivity (σ_T), grain conductivity (σ_g) e grain boundary conductivity (σ_{gb}) values (S/cm) of LLT ceramics obtained by different methods (EC, DM and EJ).

T (°C)	$\sigma_{g\,(EC)}$	$\sigma_{g(DM)}$	$\sigma_{gb\,(EC)}$	$\sigma_{T\,(EC)}$	$\sigma_{T\,(EJ)}$
25	2.84×10^{-05}	2.58×10^{-05}	3.91×10^{-08}	3.90×10^{-08}	3.76×10^{-08}
120	1.23×10^{-04}	1.15×10^{-04}	2.92×10^{-07}	2.92×10^{-07}	2.72×10^{-07}
240	5.93×10^{-04}	5.24×10^{-04}	1.22×10^{-05}	1.20×10^{-05}	1.22×10^{-05}

the simulated resistance values and the sample dimensions it was possible to evaluate the conductivity ($\boldsymbol{\sigma}$) for each region (table 1) [9, 12, 24].

As can be seen, the grain conductivity, ranging from 10^{-5} to 10^{-4} S cm^{-1}, is considerably higher than in the grain boundary region. These conductivity values are lower than that the ones shown by LLTO with concentration $x \geqslant 0.10$ [1, 6, 24]. Accordingly to Hongxia Geng [24], the higher lithium content (up to a certain saturation limit) increase the conductivity of the LLTO grain, due to the existence of a higher density of charge carriers available.

Ion conductor ceramics present blocking of charge carriers at the electrode-electrolyte interface and at the internal interfaces of the material, such as grain boundary or sample defects (internal cracks) [14]. These blockers directly affect the total conductivity of the sample, especially below a characteristic frequency, f_1. However, the blockers will have a less impact on the total conductivity as the frequency increases above f_1. In the high frequencies region the contribution to total conductivity is mainly due to the grain region [14].

The total conductivity was obtained using equation (1):

$$\sigma_T = \frac{e}{S}\left(\frac{1}{R_1 + R_2}\right) \tag{1}$$

where σ_T is the total conductivity, e the sample thickness, S the sample surface area, and R_1 and R_2 the grain and grain boundary resistance, respectively.

Another alternative path can be considered using the extended Jonscher equation (2), (JE), that represents the frequency dependence of the AC conductivity [14, 25]. Equation (2) is composed of two terms: the first describes the called 'first universality', associated with the *DC* conductivity at low frequencies and the second the beginning of the dispersion governed by the exponent n at intermediate frequencies [12, 24–26].

$$\sigma'(f) = \sigma_0\left[1 + \left(\frac{f}{f_0}\right)^n\right] + A(2\pi f)^p \tag{2}$$

On equation (2) σ_0 is the DC conductivity, f is the frequency, f_0 is the frequency at which dispersion begins, A is a temperature dependent parameter, n and p are exponential parameters, where n takes values between 0 and 1, and p is close to 1.

Figure 3 shows a log-log plot of the real part of the conductivity versus the frequency at 25 °C, 120 °C, and 240 °C. A typical behavior of ionic conductors can be observed. The red curve represents the fitting of the extended Jonscher equation to the experimental data obtained at 120 °C [27]. In the low frequencies region, an almost constant behavior is observed, which corresponds to the relaxation processes in the grain boundaries, and to the electrode ionic blockade [7]. The DC conductivity values of the LLT ceramic, obtained from equation (2), are presented in table 1.

As can be observed from figure 3, the characteristic frequency presents a dispersive behavior, which is attributed to conductive processes that occur generally in ionic conductor materials. All these processes are thermally activated and the dispersion regions move to higher frequencies with increasing temperature [7]. The dispersive regime observed at intermediate frequencies and low temperatures is often called Nearly Constant Loss (NCL). It can be seen that the slope of the dispersion decreasing as the temperature increases, due to the decrease of the NCL effect. According to Ngai [28], the NCL regime is associated with an intrinsic phenomenon dependent on Li^+ concentration at low temperatures. Funke [29] assigns the NCL behavior to local vibrations of the ions, assuming they are confined to two wells of symmetrical potentials, where the ion is free to jump between the two sites.

At high frequency, from 10^5 to 10^7 Hz, it can be observed an almost constant region which can be associated with the grain DC conductivity, wherein a long reaching movement contributes to the ionic conduction process in this material [3, 14, 29].

Figure 4 shows the normalized derivative of log(σ) versus log(f) at 25 °C, 120 °C and 240 °C (The behavior for other temperature values is similar to those shown). The 'derivative method' is an alternative way to calculate the intrinsic conductivity of the sample [14, 15]. At high frequencies region, a plateau associated with the grain DC conductivity is observed in figure 3. In fact, it is common that ionic conductors present different DC

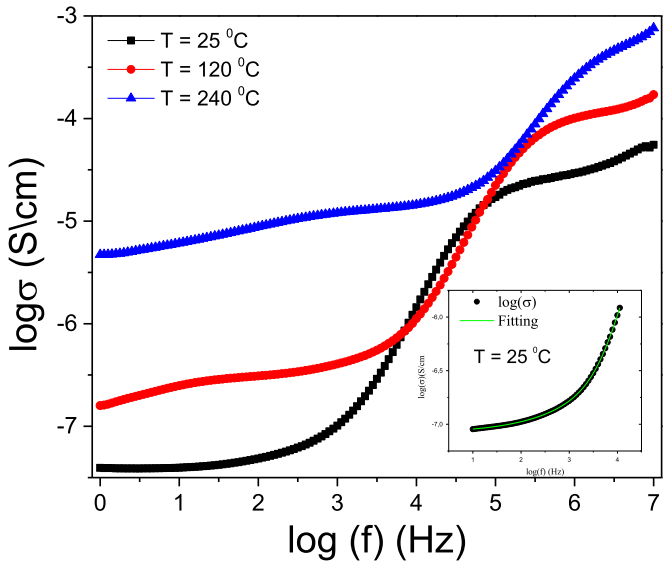

Figure 3. Log-log plot of the real part of the conductivity versus the frequency at 25 °C, 120 °C, and 240 °C. The green curve (detail) is a representative example of the fit of the JE equation to the experimental data.

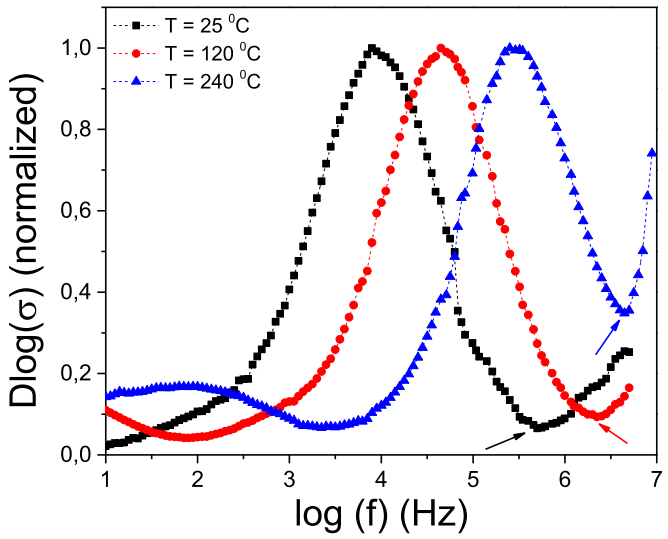

Figure 4. Normalized derivative of log(σ) versus log(f) at 25 °C, 120 °C and 240 °C. The arrows signalize the minimum of the derivative at high frequencies.

conductivity values, however in the case of LLT ceramics the DC conductivity increases with increasing frequency [28]. This behavior occurs because at high frequencies the charge carrier movement causes the maximum use of the most conductive areas of the material, i.e., grain region [29]. For this region, the derivative presents a minimum that allows evaluate the DC conductivity corresponding to the grain (arrow in figure 4).

Table 1 summarizes the conductivity values obtained by the different methods used. As can be seen, they are in good agreement with each other. Moreover, an increase of the ionic conductivity with increasing temperature is observed, revealing a thermally activated process. It is also worth to note, that in the investigated temperature range, the total conductivity values fall in the range from 10^{-8} S cm^{-1} to 10^{-5} S cm^{-1}, which can be due to the existing secondary phase, as found by DRX (figure 1(a)).

Kali [30], comparing ceramic materials obtained via SPS and conventional sintering methods, observed sample conductivity improvement when sintered via SPS. This fact was justified by the higher sample density, lower Li^+ loss, decrease of the time for the diffusion process, and consequently smaller grain size [9]. In our case, we assume that the main factor to reduce the conductivity is the presence of the $Li_4Ti_7O_{16}$ secondary phase.

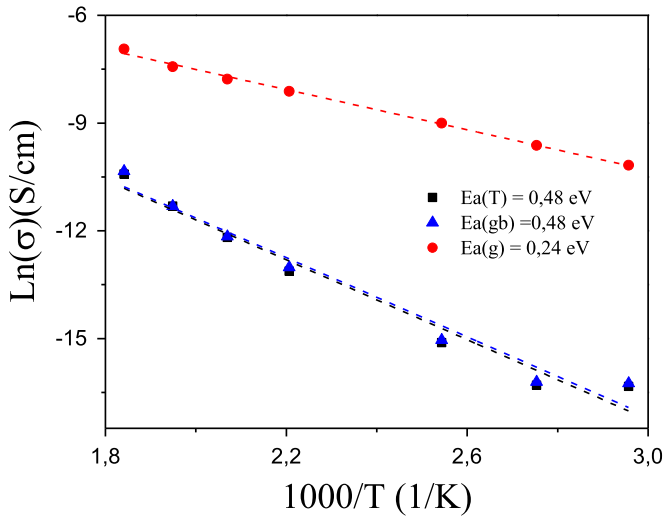

Figure 5. Inverse temperature dependence of ln(σ) for the total (T), grain (g), and grain boundary (gb) AC conductivity. The E_a values are shown in the upper corner.

A great number of Li^+ ions that could be contributing to the long-range conductive process forms the $Li_4Ti_6O_{14}$ phase, resulting in the decrease of the charge carrier density.

Figure 5 shows the inverse temperature dependence of ln(σ) for the total (T), grain (g), and grain boundary (gb) AC conductivity. The E_a values obtained are shown at the upper corner of figure 5, being similar to those previously reported [1, 10–14, 31]. This fact can be associated with the Li^+ movement, which thus stands for the main charge carrier in this material [7]. The Arrhenius behavior reveals an appreciable increase in conductivity with increasing temperature, confirming the existence of a thermally activated process. The large E_a grain boundary value indicates that there is a strong contribution of this region to block the charge carriers, thus affecting the material total conductivity. The grain activation energy is practically half of the total one. This fact can be understood by considering that the process of ionic conduction inside the grain occurs in a simpler way than in the grain boundary, wherein the impurities of the material are concentrated.

4. Conclusion

$La_{0.59}Li_{0.24}TiO_3$ ceramics, sintered through SPS, were electrically characterized at different temperatures, 25 °C to 270 °C. It was observed that the sintering method was highly efficient to obtain ceramics with good electrical properties. From the EC model analysis of the complex impedance spectroscopy data, the contributions of the DC conductivity of the grain and grain boundary were determined. The grain boundary conductivity is lower than the one found for the corresponding grain region, indicating a strong contribution of the grain boundary to block the charge carriers, thus decreasing the total conductivity of $La_{0.59}Li_{0.24}TiO_3$ ceramics. The conductivity values determined by different methods are similar, allowing us to use these methods indistinctly. From the DC conductivity obtained by the three models (EC, JE and DM) and using the Arrhenius equation, the activation energy values were calculated for the grain and grain boundary region as 0.24 eV and 0.48 eV, respectively. From these values, we conclude that the main mechanism for the conductive process in $La_{0.59}Li_{0.24}TiO_3$ ceramics concerns the movement of the Li^+ ion, which acts as the major charge carrier.

Acknowledgments

The authors would like to thank to CNPq, FAPEAM and CAPES [N° 8454/2014-00] Brazilian and FCT [938/2016] Portuguese agencies for financial support. Finally, Mrs. Inmaculada Martinez for the great help in obtaining of the samples used in this work.

ORCID iDs

Y Leyet https://orcid.org/0000-0002-5774-5391

References

[1] Yang T, Li Y and Chan C K 2015 Enhanced lithium ion conductivity in lithium lanthanum titanate solid electrolyte nanowires prepared by electrospinning *J. Power Sources* **287** 164–9

[2] Mauger A, Armand M, Julien C M and Zaghib K 2017 Challenges and issues facing lithium metal for solid-state rechargeable batteries *J. Power Sources* **353** 333–42

[3] Suk J, Lee Y H, Kim D Y, Kim D W, Cho S Y, Kim J M and Kang Y 2016 Semi-interpenetrating solid polymer electrolyte based on thiol-ene cross-linker for all-solid-state lithium batteries *J. Power Sources* **334** 154–61

[4] Wilke S, Schweitzer B, Khateeb S and Al-Hallaj S 2017 Preventing thermal runaway propagation in lithium ion battery packs using a phase change composite material: an experimental study *J. Power Sources* **340** 51–9

[5] Agrawal R C and Gupta R K 1999 Superionic solids: composite electrolyte phase - an overview *J. Mater. Sci.* **34** 1131–62

[6] Abhilash K P, Selvin P C, Nalini B, Nithyadharseni P and Pillai B C 2013 Investigations on pure and Ag doped lithium lanthanum titanate (LLTO) nanocrystalline ceramic electrolytes for rechargeable lithium-ion batteries *Ceram. Int.* **39** 947–52

[7] Deviannapoorani C, Dhivya L, Ramakumar S and Murugan R 2013 Lithium ion transport properties of high conductive tellurium substituted Li7La3Zr2O12cubic lithium garnets *J. Power Sources* **240** 18–25

[8] Tsurui T, Katsumata T and Inaguma Y 2009 Microstructural analysis of La2/3 - xLi3xTiO3single crystals and quenched samples observed by high resolution transmission electron microscopy *Solid State Ion.* **180** 607–11

[9] Mei A, Jiang Q H, Lin Y H and Nan C W 2009 Lithium lanthanum titanium oxide solid-state electrolyte by spark plasma sintering *J. Alloys Compd.* **486** 871–5

[10] Thangadurai V and Weppner W 2006 Recent progress in solid oxide and lithium ion conducting electrolytes research *Ionics (Kiel).* **12** 81–92

[11] Inaguma Y and Nakashima M 2013 A rechargeable lithium-air battery using a lithium ion-conducting lanthanum lithium titanate ceramics as an electrolyte separator *J. Power Sources* **228** 250–5

[12] Dash U *et al* 2014 Electrical properties of bulk and nano Li_2TiO_3 ceramics: a comparative study *J. Adv. Ceram.* **3** 89–97

[13] Uhlmann C, Braun P, Illig J, Weber A and Ivers-Tiffée E 2016 Interface and grain boundary resistance of a lithium lanthanum titanate ($Li_{3x}La_{2/3-x}TiO_3$, LLTO) solid electrolyte *J. Power Sources* **307** 578–86

[14] Bucheli W, Jiménez R, Sanz J and Várez A 2012 The log(σ) versus log(ω) derivative plot used to analyze the ac conductivity. application to fast Li+ion conductors with perovskite structure *Solid State Ion.* **227** 113–8

[15] Bucheli W, Arbi K, Sanz J, Nuzhnyy D, Kamba S, Várez A and Jimenez R 2014 Near constant loss regime in fast ionic conductors analyzed by impedance and NMR spectroscopies *Phys. Chem. Chem. Phys.* **16** 15346–54

[16] Moraes R S, Gonçalves A D, Stegemann C, da Silva Sobrinho A S, Miyakawa W and Massi M 2017 O_2plasma sintering study of TiO_2photoelectrodes in dye solar cells *J. Power Sources* **358** 61–8

[17] Govea-Alcaide E, Machado I F and Jardim R F 2015 10 to 25-fold increase in the transport superconducting critical current density of spark-plasma sintered Bi-2223 superconductors *J. Appl. Phys.* **117** 1–6

[18] Leyet Y, Guerrero F, Anglada-Rivera J, Martinez I, Amorin H, Romaguera-Barcelay Y, Poyato R and Gallardo-Lopez A 2016 Obtention of $Li_{3x}La_{2/3-x}TiO_3$ ceramics from amorphous nanopowders by spark plasma sintering *Ferroelectrics* **498** 62–6

[19] Bail A L 2005 Whole powder pattern decomposition methods and applications: a retrospection *Powder Diffr.* **20** 316–26

[20] Pelegov D V, Slautin B N, Gorshkov V S, Zelenovskiy P S, Kiselev E A, Kholkin A L and Shur V Y 2017 Raman spectroscopy, 'big data', and local heterogeneity of solid state synthesized lithium titanate *J. Power Sources* **346** 143–50

[21] Sanjuán M L, Laguna M A, Várez A and Sanz J 2004 Effect of quenching on structure and antiferroelectric instability of $La_{(2-x)/3}Li_xTiO_3$compounds: a raman staudy *J. Eur. Ceram. Soc.* **24** 1135–9

[22] Laguna M A, Sanjuán M L, Várez A and Sanz J 2002 Lithium dynamics and disorder effects in the Raman spectrum of $La_{(2-x)/3}Li_xTiO_3$ *Phys. Rev. B - Condens. Matter Mater. Phys.* **66** 543011–7

[23] Liang P, Yang Z and Chao X 2016 Improved dielectric properties and grain boundary response in neodymium-doped $Y_{2/3}Cu_3Ti_4O_{12}$ceramics *J. Alloys Compd.* **678** 273–83

[24] Geng H, Lan J, Mei A, Lin Y and Nan C W 2011 Effect of sintering temperature on microstructure and transport properties of $Li_{3x}La_{2/3-x}TiO_3$ with different lithium contents *Electrochim. Acta* **56** 3406–14

[25] Jonscher A K 1977 The 'universal' dielectric response *Nature* **267** 673–9

[26] MacDonald J R 2010 Addendum to 'fundamental questions relating to ion conduction in disordered solids *J. Appl. Phys.* **107** 101101

[27] Langar A, Sdiri N, Elhouichet H and Ferid M 2017 Structure and electrical characterization of ZnO-Ag phosphate glasses *Results Phys.* **7** 1022–9

[28] Ngai K L 1999 Properties of the constant loss in ionically conducting glasses, melts, and crystals *J. Chem. Phys.* **110** 10576–84

[29] Funke K 1988 Jump relaxation in solid ionic conductors *Solid State Ionics.* **28–30** 100–7

[30] Kali R and Mukhopadhyay A 2014 Spark plasma sintered/synthesized dense and nanostructured materials for solid-state Li-ion batteries: Overview and perspective *J. Power Sources* **247** 920–31

[31] Šalkus T, Kazakevičius E, Kežionis A, Orliukas A F, Badot J C and Bohnke O 2011 Determination of the non-arrhenius behaviour of the bulk conductivity of fast ionic conductors LLTO at high temperature *Solid State Ion.* **188** 69–72